Perturbing the potential vorticity field in mesoscale forecasts of two Mediterranean heavy precipitation events

By MARIA-DEL-MAR VICH[1]*, ROMUALDO ROMERO[1], EVELYNE RICHARD[2], PHILIPPE ARBOGAST[3] and KARINE MAYNARD[3], [1]Meteorology Group, Dpt. Física, Universitat de les Illes Balears, Palma de Mallorca, Spain; [2]Laboratoire d'Aérologie CNRS UMR 5560, Université de Toulouse, France; [3]Météo-France, Toulouse, France

ABSTRACT

In order to improve the quality of the Mediterranean high-impact weather (HIW) numerical predictions, this study proposes to modify the potential vorticity (PV) field of the model initial state, taking advantage of information provided by the water vapour (WV) channel of the METEOSAT-7 satellite. The implemented PV field modifications aim to reduce the mismatch between the upper-level PV features and the WV brightness temperatures guided by the known relation between these two fields (PV-WV technique). The PV-WV technique effectiveness is evaluated on two HIW events, and is also compared with two additional PV modification techniques from an earlier study. The chosen episodes occurred on 9–10 June 2000 and 9–10 October 2002 and produced heavy precipitation over both Spain and France. The main difference between these two episodes is found in the driving mechanism, a mesoscale cyclone for the June 2000 event and a larger low-pressure centre for the October 2002 case. The two additional PV modification techniques introduce perturbations along the zones highlighted by the MM5 adjoint model calculated sensitivity zones (PV-adjoint) and along the three-dimensional PV structure presenting the locally most intense values and gradients of the field (PV-gradient). A close examination of both case studies of the forecast rainfall fields and several objective verification indices show that the PV-WV technique performance exceeds the control (or non-perturbed) forecast skill while remaining inside the distribution obtained by both PV-gradient and PV-adjoint techniques. This PV-WV technique could be used to increase the ensemble spread introducing higher amplitude modifications. Thus, a more skilled ensemble prediction system could be built by taking advantage of the subjectivity inherent to this method (manual perturbations) and also of the uncertainty present in the initial state.

Keywords: PV perturbations, forecast verification, Mediterranean cyclones, METEOSAT-7 water vapour imagery, ensemble prediction systems

1. Introduction

It is well known that the uncertainty in numerical model initial conditions plays a major role in forecasting any event (Lorenz, 1963). So improving the quality of the initial condition is crucial to improving forecast performance. Extreme weather events can be especially sensitive to the uncertainties of the atmospheric state. Many studies have shown that enhancing initial condition accuracy results in a better forecast (Rabier et al., 1996; Nutter et al., 1998;

Romero et al., 2000; Homar et al., 2003; Nuissier et al., 2007). One approach to improving the initial state quality is to modify the atmospheric fields within the possible range of states of the atmosphere to get closer to the true state. A similar approach is used in ensemble forecasting that aims to approximate the probability density function (PDF) of atmospheric initial states and propagate it forward in time with a numerical weather model in order to predict the PDF of the atmosphere state at a future time.

This study implements a method to improve the quality of the initial conditions by modifying them using satellite observational data for guidance. The method (see Argence et al., 2009) takes advantage of the relationship

*Corresponding author.
email: mar.vich@uib.es

1

between potential vorticity (PV) field and water vapour (WV) imagery. The WV absorption bands, obtained by a geostationary satellite like the METEOSAT-7, are sensitive to the profiles of temperature and humidity, specially at tropopause level. Therefore, it is possible to relate the WV brightness temperature (grey tones, in the images) to relevant PV anomalies, under some assumptions. So, if the PV field of the analyses (a surrogate of the initial conditions according to the invertibility principle; Hoskins et al., 1985) does not properly match the WV images, the PV field is modified to avoid the mismatch (a procedure called *PV-WV technique* from now on).

Many studies have already highlighted the sensitivity of forecasts to PV modifications (e.g. Huo et al., 1999; Homar et al., 2003; Romero, 2008). Moreover, Vich et al. (2011a, 2011b) present two ensemble prediction systems (EPSs) based on perturbing the initial and boundary conditions of the MM5 PV field. The PV perturbations are set from a PV error climatology that characterizes typical PV errors in the ECMWF nesting data, both in intensity and displacement. The intensity and displacement perturbation magnitudes of the PV field are chosen randomly from this climatology, while the location is given by the *perturbation zones* defined by each ensemble generation method. Both ensembles exhibit greater forecasting skill than a multiphysics EPS and a deterministic run when tested within a collection of high-impact MEDEX (Mediterranean Experiment on cyclones that produce high-impact weather in the Mediterranean, a project endorsed by the WMO under the THORPEX WWRP, http://medex.aemet.uib.es. cyclonic episodes; Vich et al., 2011a, 2011b). Other studies that focus on modifying the PV field according to WV imagery show its positive effect on reducing forecast error (e.g. Dermitas and Thorpe, 1999; Hello and Arbogast, 2004; Guérin et al., 2006; Røsting and Kristjánson, 2006, 2008; Manders et al., 2007; Argence et al., 2009).

This paper evaluates the forecast results obtained using the PV-WV technique when applied to two different Mediterranean high-impact weather (HIW) events. Specifically, several verification scores, like ROC curves or Taylor diagrams, will evaluate the performance of the technique using the 9–10 June 2000 and 9–10 October 2002 events, both from the MEDEX database. Additionally, the PV modification techniques used on the two EPSs shown in the study of Vich et al. (2011a, 2011b) represent a remarkable benchmark to compare with the PV-WV technique used in this study.

A description of the two MEDEX events used as testbed can be found in Section 2. Section 3 deals with the procedure and application of all three PV modification techniques in detail. The results are examined in Section 4.

Finally, concluding remarks and future outlooks are presented in Section 5.

2. Meteorological description of the events

This study targets the 9–10 June 2000 and 9–10 October 2002 HIW events collected from the MEDEX database. Both events produced large amounts of precipitation over Spain and France, up to 223 and 200 mm 24-h accumulated rainfall, respectively, and presented similar synoptic situations.

The event of 9–10 June 2000 (Fig. 1) was characterised by the entrance of an Atlantic low-level cold front and an upper-level trough that contributed to the generation of a mesoscale cyclone in the Mediterranean Sea along the Catalonia Coast (northeast Spain). The circulation associated with this mesoscale cyclone advected warm, moist air towards Catalonia from the Mediterranean Sea. The combination of the Mediterranean air mass at low levels with the cold air aloft is seen in Fig. 1b and d as moderate values of convective instability along the Spanish Mediterranean coast. The cyclone-induced maritime flow together with the prominent orography of northeast Spain produced strong convergence of the water vapour flux in the lower troposphere during the whole episode (same figures). As a result of this favourable synoptic-mesoscale environment, two long-lived mesoscale convective systems developed over Catalonia and later merged and remained quasistationary near Barcelona city for nearly two hours. A more detailed diagnostic description of the event, including a sequence of radar images, can be found in the study of Martín et al. (2007). A comparison of the control simulation (initialised using ECMWF 24-h forecasts; Fig. 1) with the ECMWF analyses performed at the same time is shown in Fig. 2. Significant differences in the sea level pressure field can be observed over eastern Spain and the western Mediterranean area, i.e. downstream from the upper-level trough. Specifically, the simulation shows a northward displacement of the western Mediterranean low in such a way that by the time of the flash floods (early on 10 June) the cyclone is already centred over Catalonia. This surface effect is consistent with a further extension of the upper-level PV anomaly into northeast Spain (Fig. 2d).

Although the event of 9–10 October 2002 (Fig. 3) shares many large-scale characteristics with the 2000 event, some remarkable differences can be highlighted. For example, the upper-level trough has a longer wave length and remains negatively tilted with respect to the horizontal wind shear during the episode, the surface low-pressure area is much larger, spreading over the whole western Mediterranean, and its minimum is located farther north (Fig. 3a and c). The resulting maritime flow and thermal
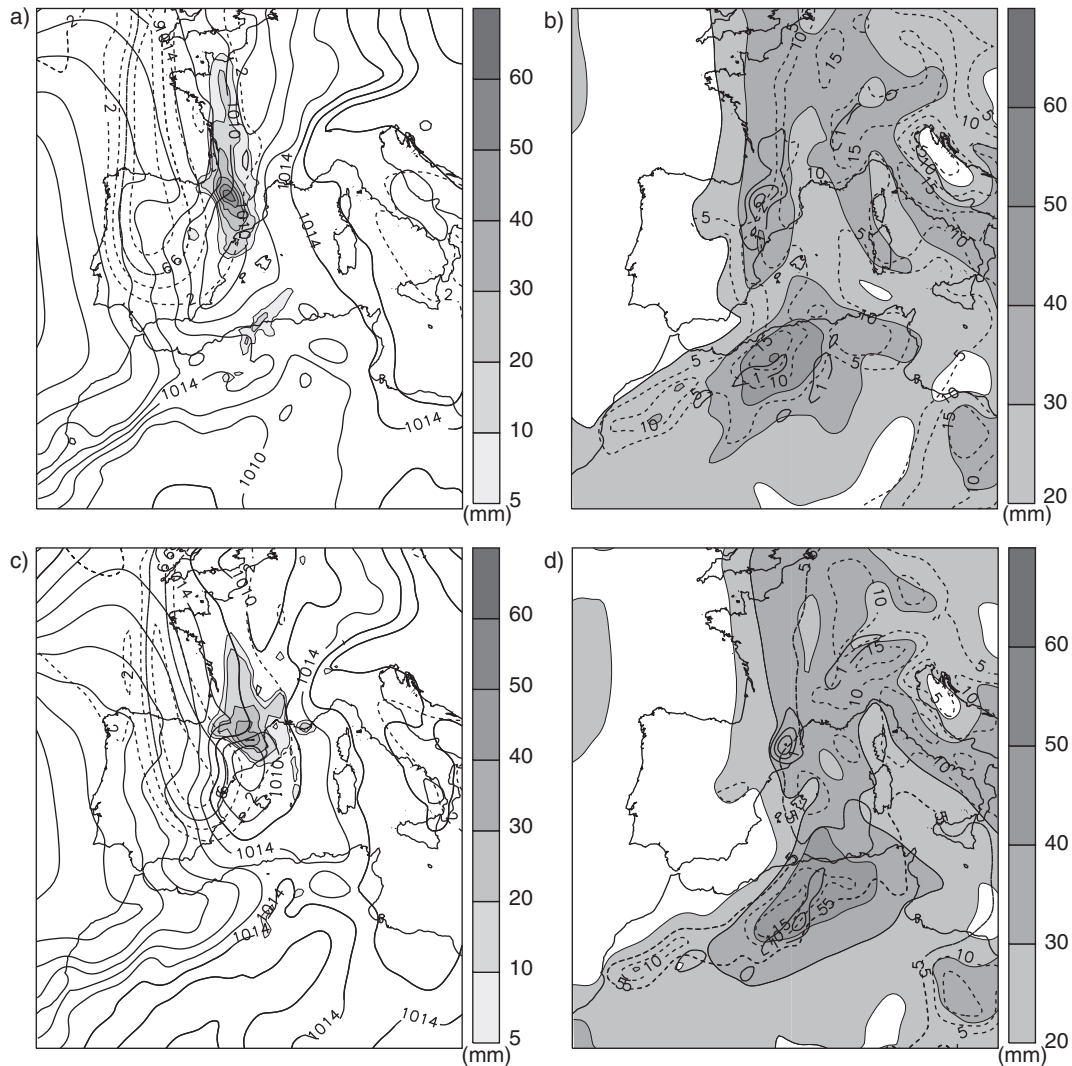
Fig. 1. MM5 control forecast from 00 UTC 9 June to 06 UTC 11 June 2000 initialised using ECMWF 24-h forecasts. (Left) Potential vorticity on the 330 K isentropic surface (dashed line, in PV units), sea level pressure (continuous line, in hPa) and 6-h accumulated rainfall (shaded contours, in mm according to scale) on (a) 9 June at 18 UTC and (c) 10 June at 00 UTC. (Right) Water vapour flux convergence in the 1000–700 hPa (continuous line, contour interval is $1 \text{ g}^{-2}\text{s}^{-1}$, starting at $1 \text{ g}^{-2}\text{s}^{-1}$), convective instability (as measured by the equivalent potential temperature difference between 1000 and 500 hPa, at intervals of $5\,°\text{C}$ starting at $5\,°\text{C}$; dashed line) and precipitable water (shaded contours, in mm according to scale) on (b) 9 June at 18 UTC and (d) 10 June at 00 UTC.

advection over the Catalan coast are weaker, but the impinging Mediterranean winds over the south coast of France, in the form of a well-defined low-level jet (LLJ), are more notable. The diagnostic indicators shown in Fig. 3b and d evidence that, with respect to the previous event, basic ingredients for deep moist convection (large precipitable water, convective instability and low-tropospheric water vapour flux convergence) are shifted towards the northeast in this case, affecting mainly the south coast of France. Compared against the ECMWF analyses (Fig. 4), in this case, the mesoscale simulation produces a deeper Mediterranean cyclone with larger

pressure gradient along its eastern flank, thus leading to a stronger LLJ than in the analyses.

3. PV modifications methodology

3.1. Satellite-based modifications

The PV field is a useful meteorological parameter to study the dynamical structures at the synoptic scale, thanks to the conservative and invertibility principles (Hoskins et al., 1985). In fact, both principles make the PV field a suitable tracer of upper-level dynamics, which plays an important
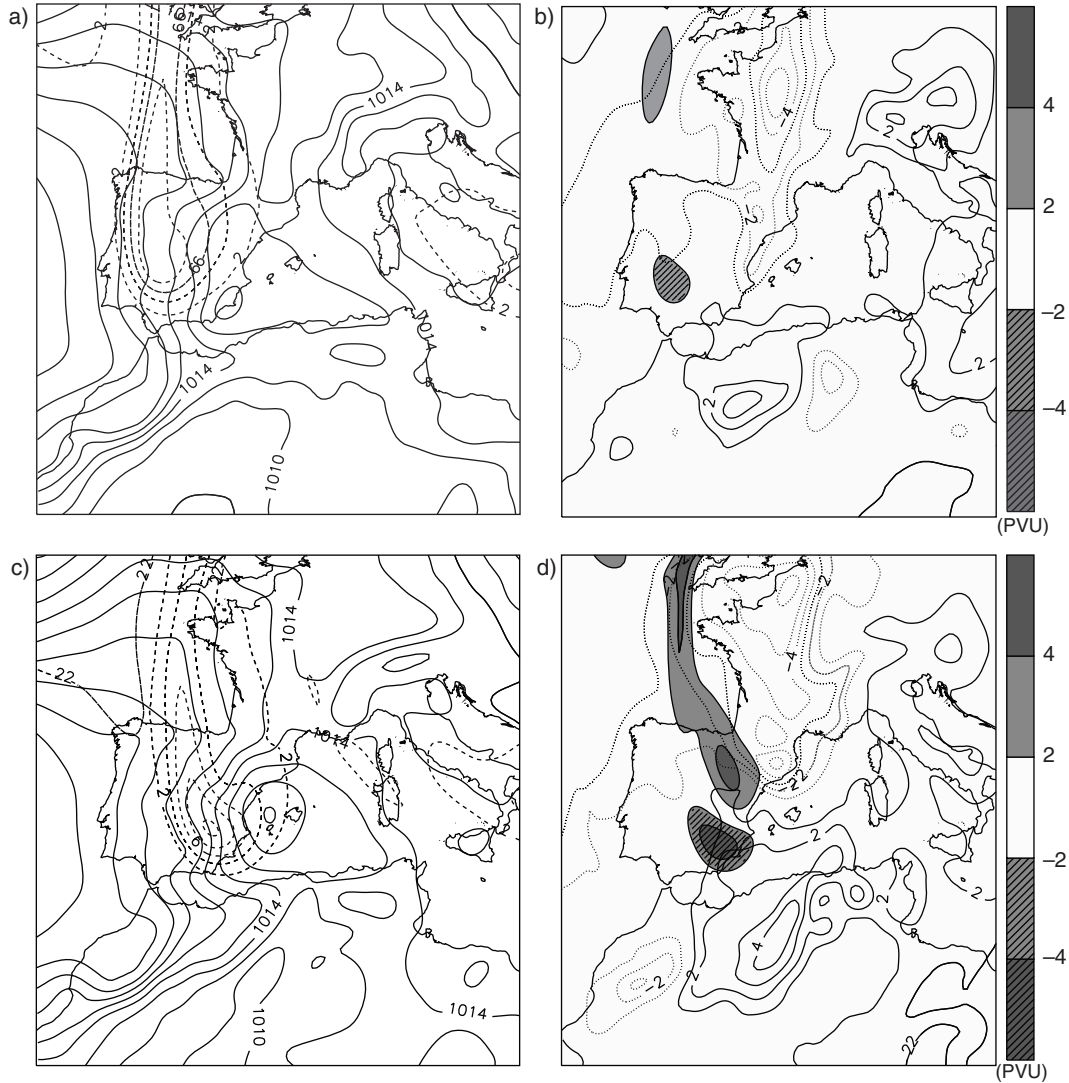
Fig. 2. Comparison of MM5 control forecast against ECMWF analyses for the June 2000 event. (Left) Potential vorticity on the 330 K isentropic surface (dashed line, in PV units) and sea level pressure (continuous line, in hPa) on (a) 9 June at 18 UTC and (c) 10 June at 00 UTC, according to the analyses. (Right) Differences between the corresponding MM5 control forecast and the analyses for the potential vorticity on the 330 K isentropic surface (shaded contours plain/patterned for positive/negative values, in PV units according to scale) and sea level pressure (continuous/dashed line for positive/negative values, in hPa) on (b) 9 June at 18 UTC and (d) 10 June at 00 UTC.

role in mid-latitude synoptic developments. Upper-level positive PV anomalies can be interpreted as upper-level disturbances penetrating into the upper troposphere linked to the undulation of the tropopause. As Santurette and Joly (2002) showed, only one level of the dynamical tropopause is needed to diagnose upper-level dynamics if balance in the atmosphere and a monotonic vertical PV gradient are assumed, generally the 1.5 PVU surface (1 PVU = 10^{-6} m^2 s^{-1} K kg^{-1}) or the PV field on an isobaric surface between 200 and 400 hPa.

The water vapour imagery provided by the 6.3-μm METEOSAT-7 channel is an important tool for synoptic-scale analyses as it mostly reveals the WV content in the mid- and upper troposphere. Because there is a close relationship between PV distribution and satellite WV images in dynamically active regions, their joint examination provides an excellent framework to asses numerical model behaviour and/or the quality of analyses. The key point to our PV-WV technique is that the dark (light) features in the WV images can be associated to positive (negative) PV anomalies, descending (ascending) motions and low (high) geopotential heights of the dynamical tropopause. Santurette and Georgiev (2005) detail the use of WV imagery side-by-side with the PV
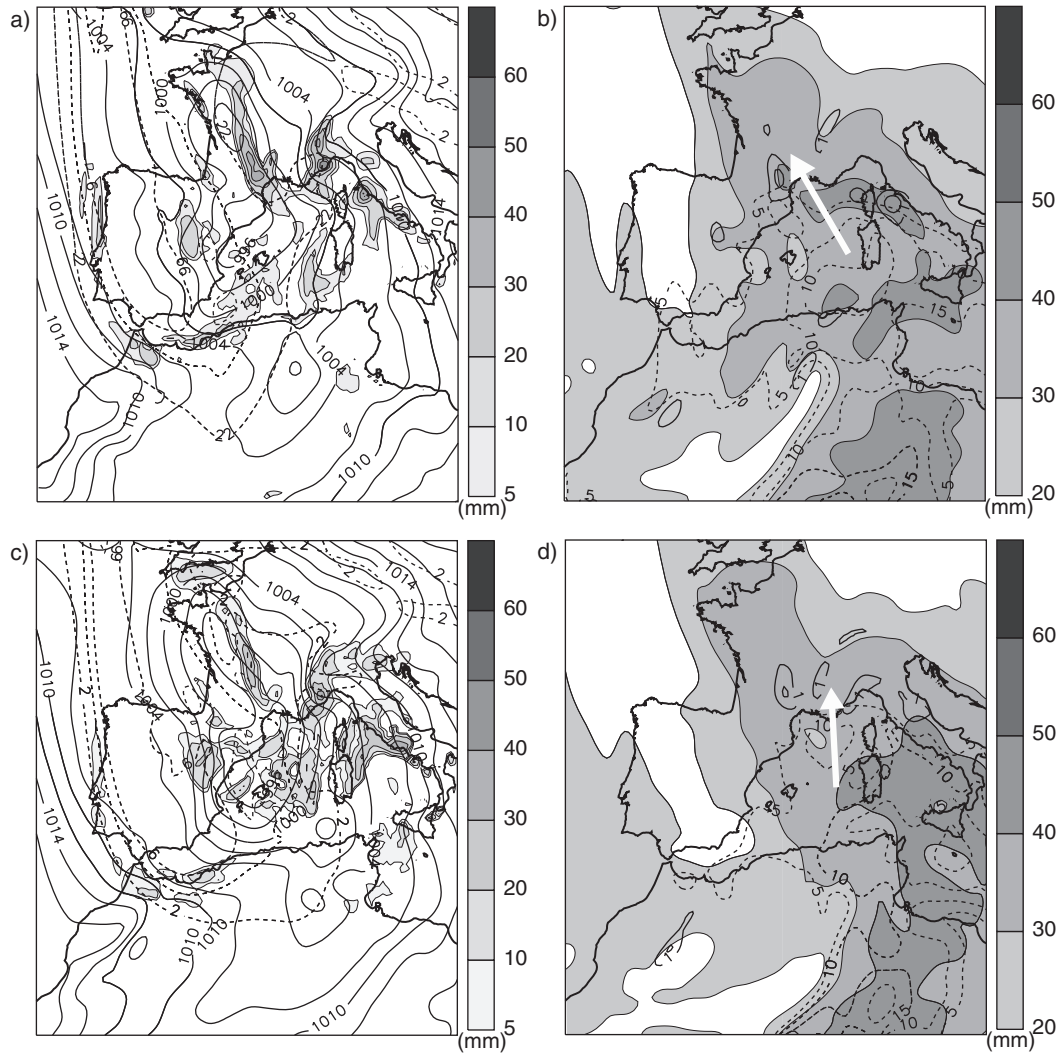
Fig. 3. Same fields as shown in Fig. 1, except for the MM5 control forecast from 00 UTC 9 October to 06 UTC 11 October 2002. (a and b) 9 October at 18 UTC and (c and d) 10 October at 00 UTC. The arrows in (b) and (d) denote the position and direction of the low-level jet (LLJ).

field, as well as a thorough analysis of both of them independently.

Taking advantage of the known relationship between the METEOSAT-7 WV images and the PV field close to the dynamic tropopause level, some modifications can be applied to the PV field in the analyses to improve their matching. These modifications are applied to the dynamical tropopause surface defined by the height of the 1.5 PVU surface. Following the procedure used in the study by Argence et al. (2009) and Arbogast, Maynard, and Fougère-Piriou (2012), these steps are followed:

- Compare the dynamical tropopause (1.5 PVU surface height) with the METEOSAT-7 WV brightness temperature distribution at the simulation initial time.
- Reduce the mismatch by modifying the topography of the dynamical tropopause accordingly.
- For each horizontal grid point, the new vertical height of the dynamical tropopause defines a PV correction which is actually the difference between the original PV value at that height and 1.5 PVU. A 1DVAR method based on known forecast error statistics is then applied to build a vertical profile of PV modification over the corresponding grid point.
- Invert the modified and control (unmodified) PV fields given the mass–wind balance condition derived by Charney (1955) following the methodology presented by Romero (2001).
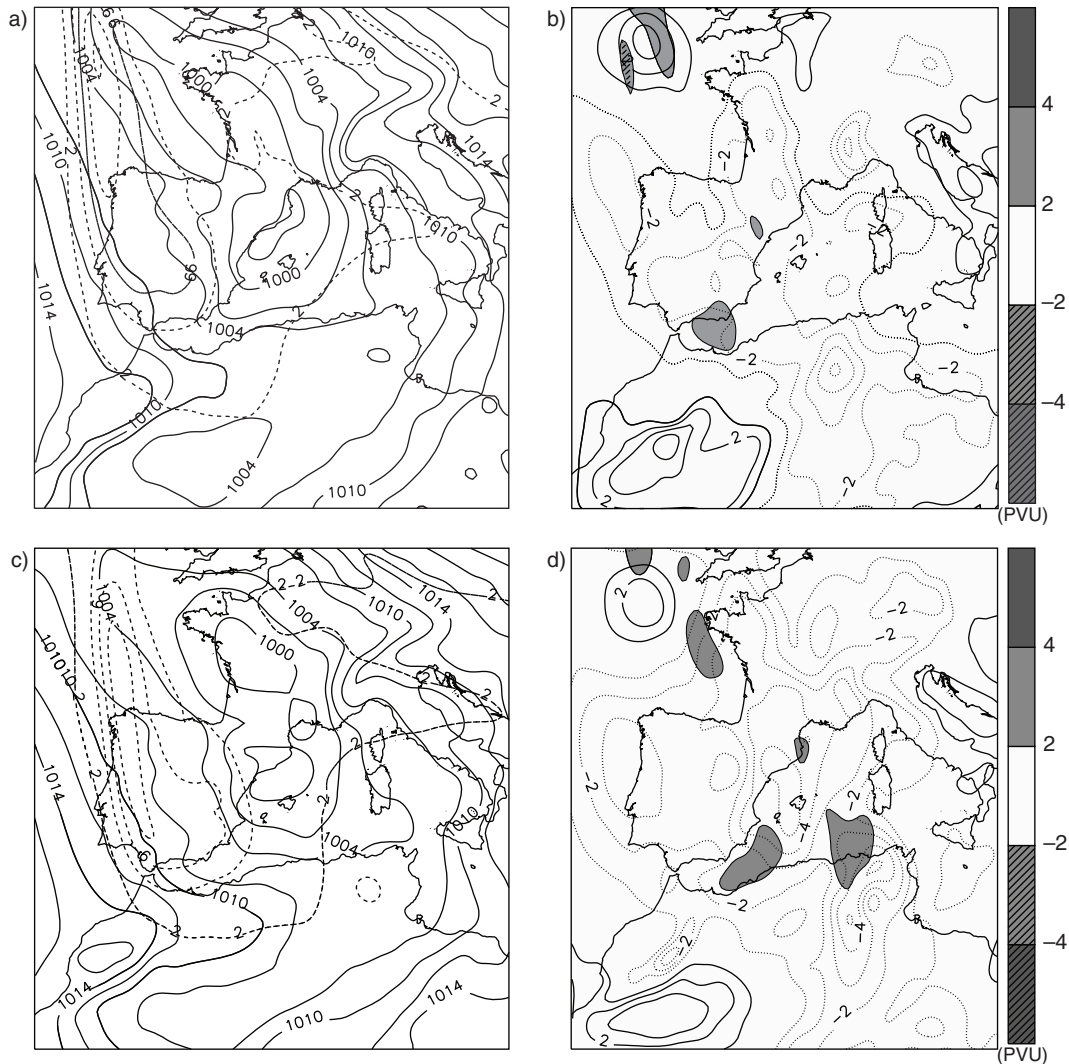
Fig. 4. Same fields as shown in Fig. 2, except for the October 2002 event. (a and b) 9 October at 18 UTC and (c and d) 10 October at 00 UTC.

- Identify the initial perturbation as the difference between the PV-control and PV-modified inverted fields.
- Calculate the perturbed atmospheric state by adding this perturbation to the original model initial conditions.
- Perform the corresponding numerical run using this *improved* initial state.

The PV field modifications consist of adding/subtracting PV structures as well as shifting them to minimise the mismatch between the PV field and the WV brightness temperature. It is also worth to note that these modifications are confined to the layer between 150 and 500 hPa to target the corrections on the tropopause topography.

A practical implementation of the presented technique is illustrated in Fig. 5. It shows the comparison of the METEOSAT-7 WV brightness temperature and the PV field at 300 hPa for the initial time of the June 2000 case, calculated using the ECMWF analysis, as well as the corresponding perturbed PV field. Using the known relationship between WV and PV, one can decide how to modify the unperturbed PV field to reduce the mismatch. The locations of these modifications are indicated in Fig. 5 by capital letters, where G means that the original PV gradient has been increased and C that the curvature has been strengthened to match the curvature of the PV feature present on the WV image. The resulting perturbed PV field agrees much better with the WV brightness temperature field (dashed contours in the same figure). An equivalent procedure has been done on the initial state of the October
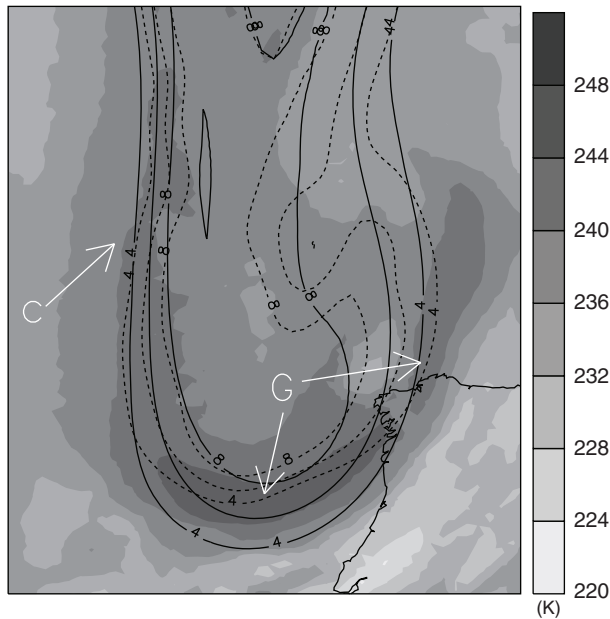
Fig. 5. Overlay for 9 June 2000 at 00 UTC of the potential vorticity field at 300 hPa unperturbed and perturbed (solid and dashed lines, respectively, contour interval 2 PVU, above 4 PVU) and METEOSAT-7 water vapour brightness temperatures (shading, in K according to scale). The letters G and C indicate the locations where the PV modifications are applied (see the details in the text).

2002 case (not shown). Santurette and Joly (2002) offer an excellent guide on how to perturb the PV field in this context and provide several practical examples.

3.2. Alternative PV modification techniques

Two additional PV modification methods taken from the work of Vich et al. (2011a, 2011b) are used to generate ensemble predictions of the case studies by perturbing the model initial and boundary conditions. The perturbations are applied over the PV field, exploiting the connection between PV anomalies and cyclones. Working with the PV field has the advantage of defining the perturbations on a single variable, while the PV inversion technique ensures that the basic-state meteorological fields (temperature and wind) are consistently perturbed without compromising the mass–wind balance of the atmosphere, as in the PV-WV technique.

These ensembles are called PV-gradient and PV-adjoint in reference to the criteria used to locate the perturbing PV zones. The PV-gradient adopts the zones of the most intense values and gradients of the PV field as the most sensitive areas of the subsequent cyclogenesis process (Romero et al., 2006; Garcies and Homar, 2009). On the other hand, the PV-adjoint uses the PV sensitivity field

calculated with the MM5 adjoint model under a response function defined by the surface vorticity field averaged over the targeted cyclone. Previous studies (e.g. Homar and Stensrud, 2004; Homar et al., 2006) have already used this type of objectively-obtained zones as an appropriate proxy of cyclone sensitivities.

With regard to the PV modifications, both methods use a PV error climatology to avoid unrealistic perturbations. This climatology provides a PV perturbation range consistent with the actual PV field uncertainties in order to randomly increase/decrease the PV field intensity and displace its features on the regions highlighted by each method. Both ensembles proved to be skilful when tested for the precipitation field over 19 MEDEX cyclonic episodes, even though the PV-gradient ensemble was generally better than the more computationally expensive PV-adjoint EPS (see details in the study by Vich et al., 2011a, 2011b).

4. Results examination

Once the agreement between the PV field and WV brightness temperatures has been strengthened by modifying the PV field accordingly, this modified field is incorporated into the model initial state using the PV inversion technique cited before. Then two forecasts per event are run, the non-perturbed and perturbed, using the following MM5 configuration: a simulation domain (Fig. 1) defined over a grid mesh made up of 30 sigma levels on the vertical and 120×120 nodes with a 22.5-km resolution on the horizontal, while the model physical parameterisation set consists of the explicit moisture scheme of Reisner graupel (Reisner et al., 1998), the cumulus parameterisation scheme of Kain-Fritsch 2 (Kain, 2004), the PBL scheme of MRF (Troen and Mahrt, 1986; Hong and Pan, 1996), the cloud radiation scheme of Dudhia (1989) and the five-layer soil model described by Dudhia (1996). The model runs are nested in the ECMWF 24-h forecasts with the aim of emulating the forecasting system of the UIB Meteorology Group (see http://mm5forecasts.uib.es). This type of nesting is necessary due to the computational limitations of the Group, which prevent a feasible implementation of a forecasting system based on real-time analyses. Specifically, the MM5 model is run every day, initialised with global coarse resolution, 24-h forecast fields valid at 00 UTC, the next day and forced at the lateral boundaries with the subsequent data (i.e. with 30, 36, ..., 72 h global forecasts), using the same model configuration described above. In this sense, the 24-h forecasts used here represent a quasi-operational benchmark test. The simulations start at 00 UTC on 9 June 2000 and at 00 UTC on 9 October 2002 with a lead time of 54 h to make the comparison with observations easier, as the used raingauge data corresponds

to 24-h accumulated precipitation, from 06 UTC to 06 UTC the next day. These observations come from the climatological raingauge networks maintained by Météo-France and AEMET (Agencia Estatal de Meteorología – Spanish Weather Service).

It is worth noting that this study does not take the model uncertainties into account, particularly those due to the physical parameterisation schemes, that is, we focus only on the initial condition uncertainty while assuming a perfect model. Previous studies (e.g. Houtekamer et al., 1996; Stensrud et al., 1999; Vich et al., 2011a) have exploited the known impact of model physical parameterisation on precipitation distribution to design multiphysics ensemble prediction systems. Although Vich et al. (2011a)

concluded that the PV-gradient EPS outperforms a multi-physics EPS for Mediterranean heavy precipitation situations, the potential of a hybrid approach where different physical schemes are introduced after perturbing the initial state (e.g. Meng and Zhang, 2007) would be worth exploring.

The results obtained after implementing the PV modifications are shown in Fig. 6 for the June 2000 case and in Fig. 7 for the October 2002 case. For example, in comparison with Fig. 1a–c, Fig. 6a–c shows that the progression towards the east and northeast of the PV anomaly associated with the upper-level trough is slower (note the dipole structure for the PV difference field shown in Fig. 6b–d), as well as the resulting shallower and slower
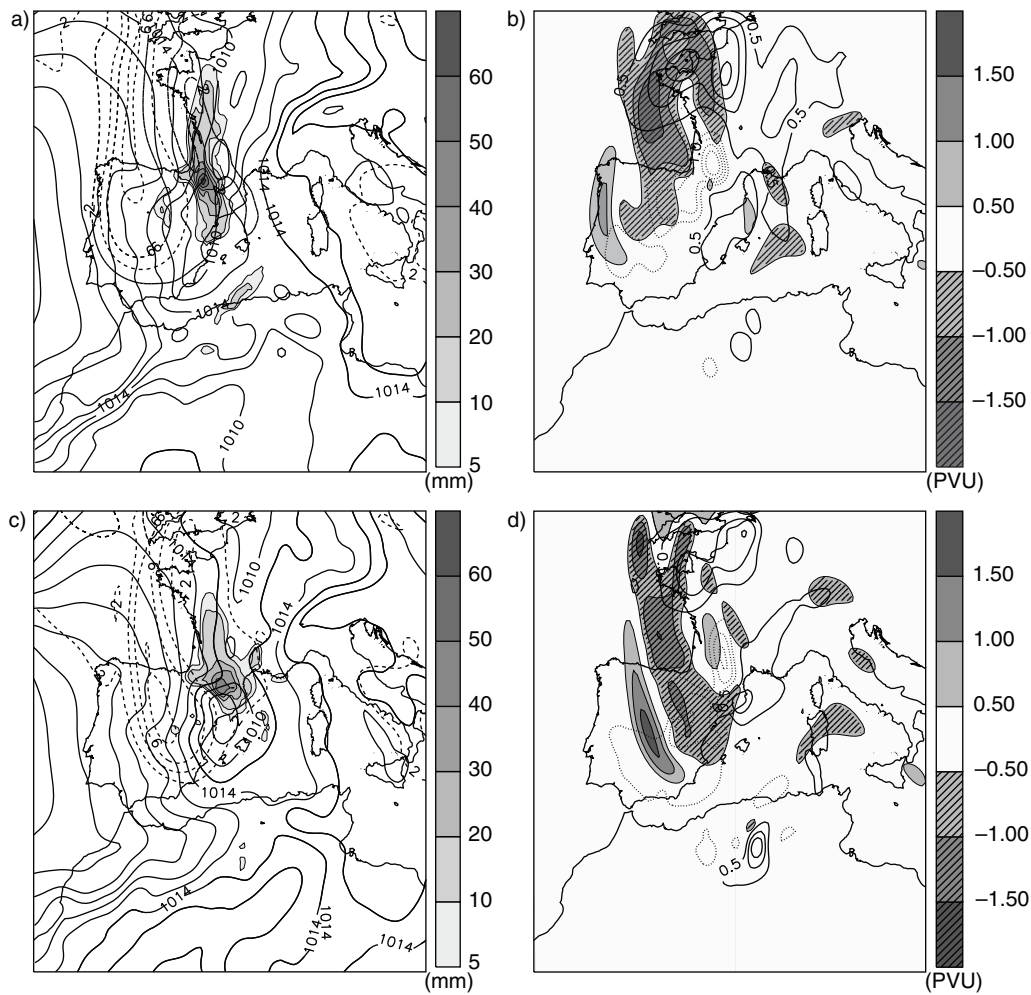

Fig. 6. MM5 perturbed forecast, once the potential vorticity modifications are applied, from 00 UTC 9 June to 06 UTC 11 June 2000. (Left) Potential vorticity on the 330 K isentropic surface (dashed line, in PV units), sea level pressure (continuous line, in hPa), and 6-h accumulated rainfall (shaded contours, in mm according to scale) on (a) 9 June at 18 UTC and (c) 10 June at 00 UTC. (Right) Differences between the MM5 perturbed forecast and the corresponding MM5 control forecast (shown in Fig. 1) for the potential vorticity on the 330 K isentropic surface (shaded contours plain/patterned for positive/negative values, in PV units according to scale) and sea level pressure (continuous/dashed line for positive/negative values, in hPa) on (b) 9 June at 18 UTC and (d) 10 June at 00 UTC.
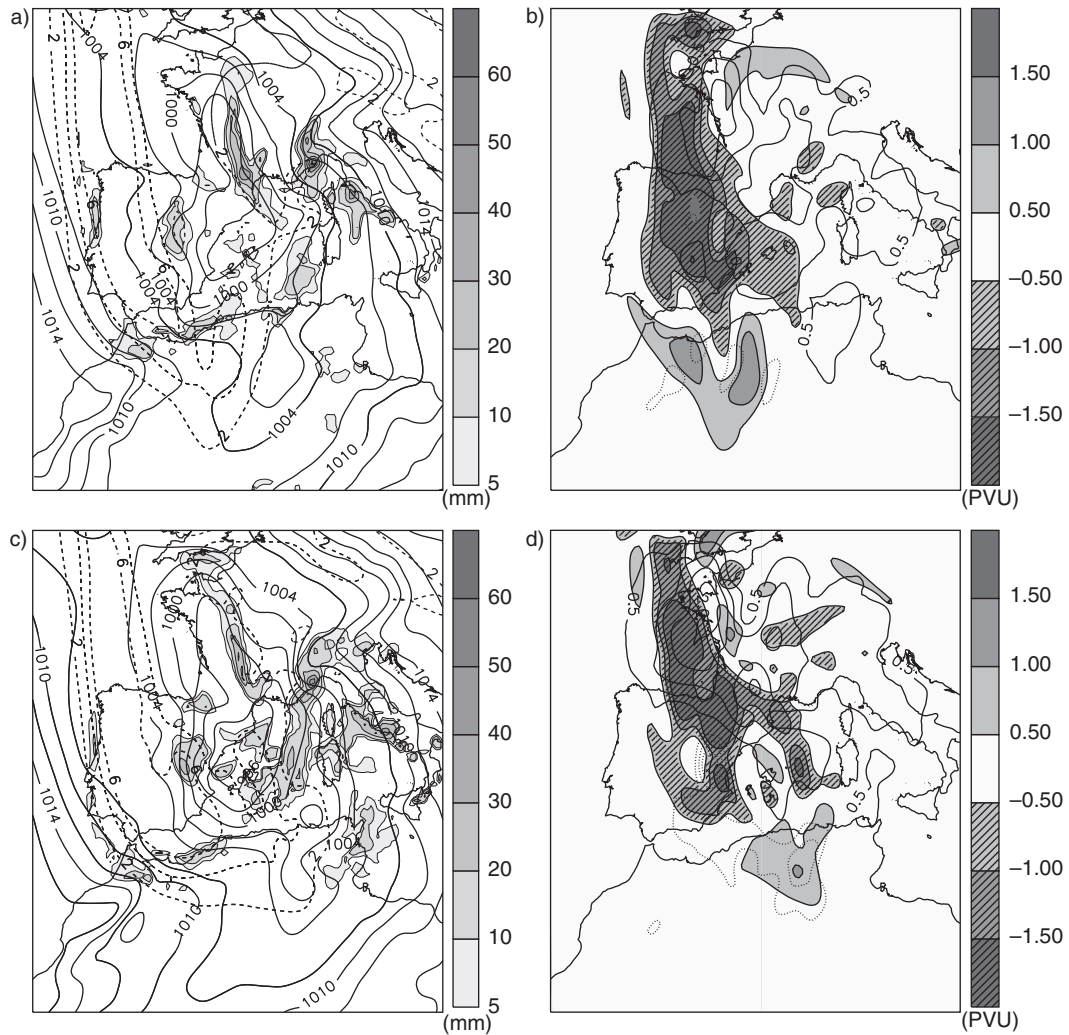
Fig. 7. Same fields as shown in Fig. 6, except for the October 2002 event. (a and b) 9 October at 18 UTC and (c and d) 10 October at 00 UTC.

surface cyclone over the Spanish coast (same figures). Although these changes could be considered irrelevant, and, in fact, the meteorological scenario has been essentially unaltered at synoptic scale, the mesoscale details do have a tangible impact on the forecast precipitation (see Fig. 8). Comparatively, the PV modifications dictated by the PV-WV visual mismatch in the October 2002 case are larger (compare the evolution shown in Fig. 7a–c with the sequence shown in Fig. 3a–c, and the difference is shown in Fig. 7b–d), but the resulting precipitation forecast turns to be less sensitive to the initial state perturbation (Fig. 9). These results are consistent with the findings of Romero et al. (2005) who, based on perturbed numerical simulation of Mediterranean heavy precipitation events, concluded that cases driven by sub-synoptic cyclones (like the June 2000 event) are more sensitive to the uncertainties of the precursor upper level disturbance than those cases gov-

erned by a Mediterranean LLJ embedded in a large-scale low (e.g. October 2002).

Figures 8 and 9 show the 30–54 h forecast accumulated rainfall for the non-perturbed and perturbed runs and the corresponding observation, for each case. The perturbed simulation of both cases presents a forecast rainfall field closer to the observed field than the non-perturbed one, even though it does not completely match the observed pattern. A closer examination shows that the highest rainfall value for the June 2000 case predicted by the perturbed run is located farther southeastward than in the non-perturbed forecast and nearer to the observed maximum (Fig. 8). A similar affirmation is true for the October 2002 case (Fig. 9), where the maximum rainfall centre (southern tip of the French Riviera) from the perturbed run is shifted northwestwards with respect to the non-perturbed and nearer to the observed maximum.
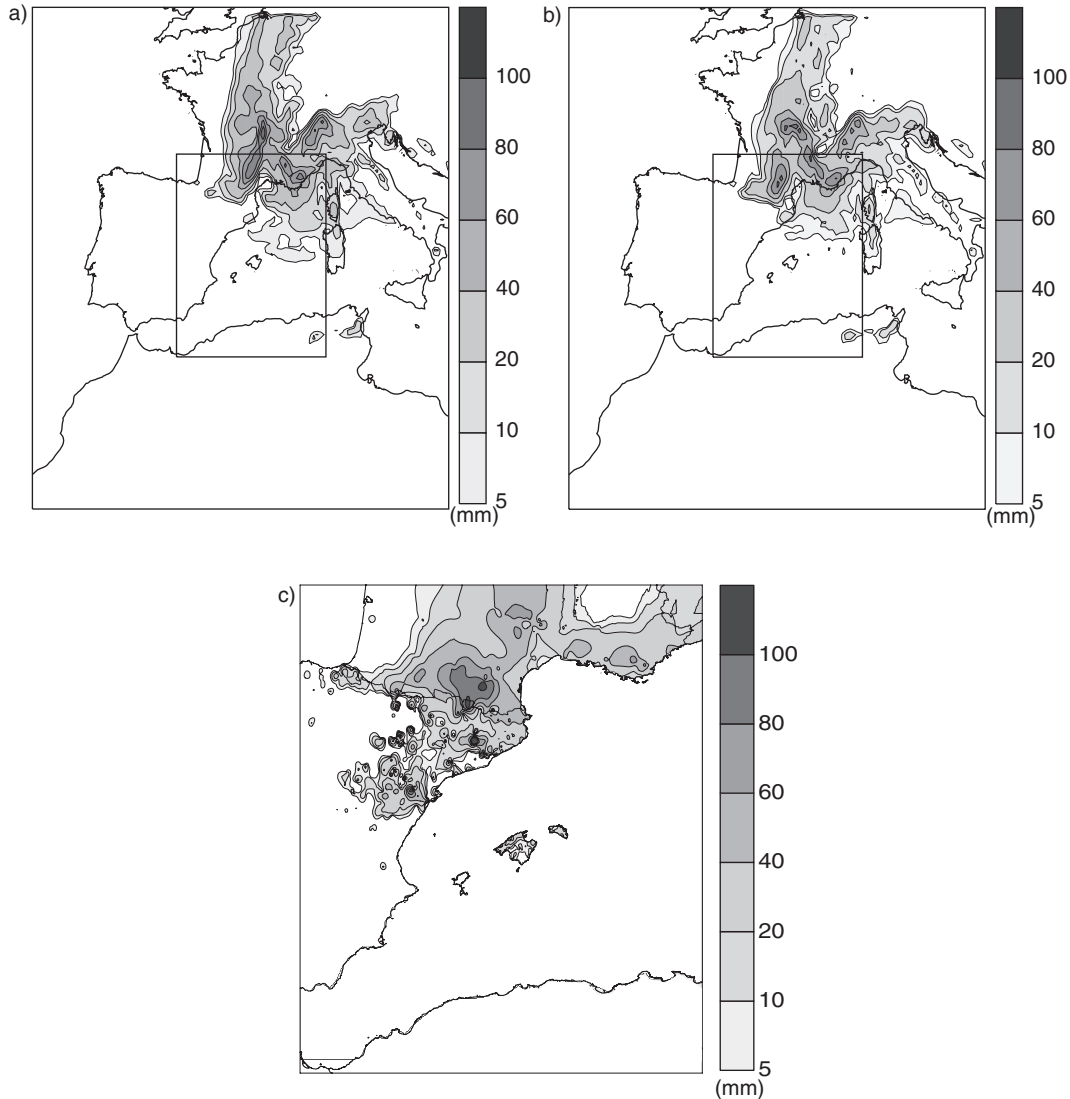
Fig. 8. Accumulated rainfall (shaded, in mm according to scale) between 10 June 2000 at 06 UTC and 11 June 2000 at 06 UTC. (a) Non-perturbed run, (b) PV-WV run and (c) observed.

A different approach for evaluating the improvement accomplished by the PV-WV technique is to use objective verification scores and compare their values with the results obtained for the same case studies by the EPSs based on the alternative PV modification techniques presented in Section 3.2.

The ROC curve (Mason, 1982) alludes to the ability of the forecast to discriminate between events and non-events and plots the probability of detection against probability of false detection. The forecast discriminating skill given by the ROC curve can be summarised in a single value, focusing on the area under the obtained curve (ROC area). As a matter of fact, an ROC area of 0.5 indicates no skill above a random prediction and 1 a perfect skill. The ROC

areas obtained using the PV-WV technique and the two ensembles for both case studies (Fig. 10) are very skillful, because all forecasts lie well above 0.7, the threshold established by Stensrud and Yussouf (2007) to indicate the usefulness of a forecasting system. Moreover, on both events, the non-perturbed and the PV-WV perturbed runs lie within the range of both ensembles, the perturbed one being more skilled than the non-perturbed run, especially for the 2000 event. It is worth mentioning that these results correspond to the 30–54 h forecast accumulated rainfall, but analogous results were found for the 06–30 h forecast period (not shown). The same behaviour was observed for the rest of verification scores explored, therefore only the 30–54 h rainfall verification results are shown.
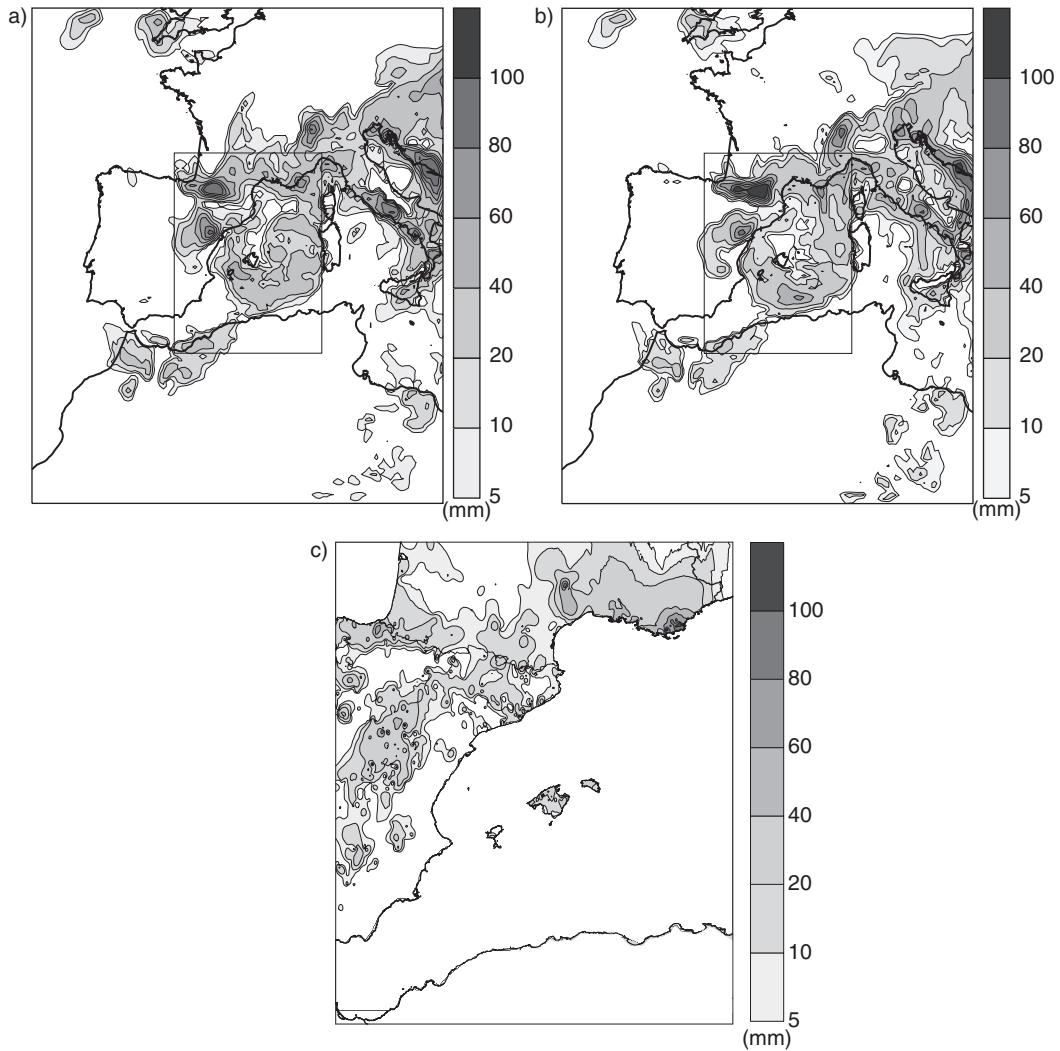
Fig. 9. Accumulated rainfall (shaded, in mm according to scale) between 10 October 2002 at 06 UTC and 11 October 2002 at 06 UTC. (a) Non-perturbed, (b) PV-WV run and (c) observed.

The Q-Q plots are a useful tool to compare the observed and forecast distributions in terms of quantiles. The diagonal line represents the perfect score, and the region below (above) the diagonal indicates that the forecast underestimates (overestimates) the observation. A more detailed description on a large collection of verification scores, Q-Q plots included, can be found in the study of Wilks (1995). The results (Fig. 11) show that, as in the ROC area results, the non-perturbed and the PV-WV perturbed runs lie within the range of both ensembles, with the perturbed forecast being more skilled than the non-perturbed run. Each event falls into a different region of the diagram, the June 2000 case underpredicts the observed precipitation while the October 2002 case tends to overpredict it.

The Taylor diagram graphically shows several statistics useful to determine model performance in a single diagram (Taylor, 2001). The plotted statistics are the correlation coefficient and the centred pattern root-mean-square (RMS) difference between the forecast and the observed field, and the standard deviation of both fields. The diagram does not provide information about overall biases but only characterises the centred pattern error, as the means of the fields have been subtracted.

The diagram of the June 2000 event (Fig. 12a) shows the same tendency seen in other verification scores, i.e. the non-perturbed and the PV-WV perturbed results are contained within both the ensembles' results. This behaviour is also observed for the October 2002 (Fig. 12b) PV-WV perturbed run while the non-perturbed run lies on the edge of the distribution. One of the differences between the two events is the pattern displayed by the whole collection of runs in the Taylor diagram; the June 2000 pattern is more
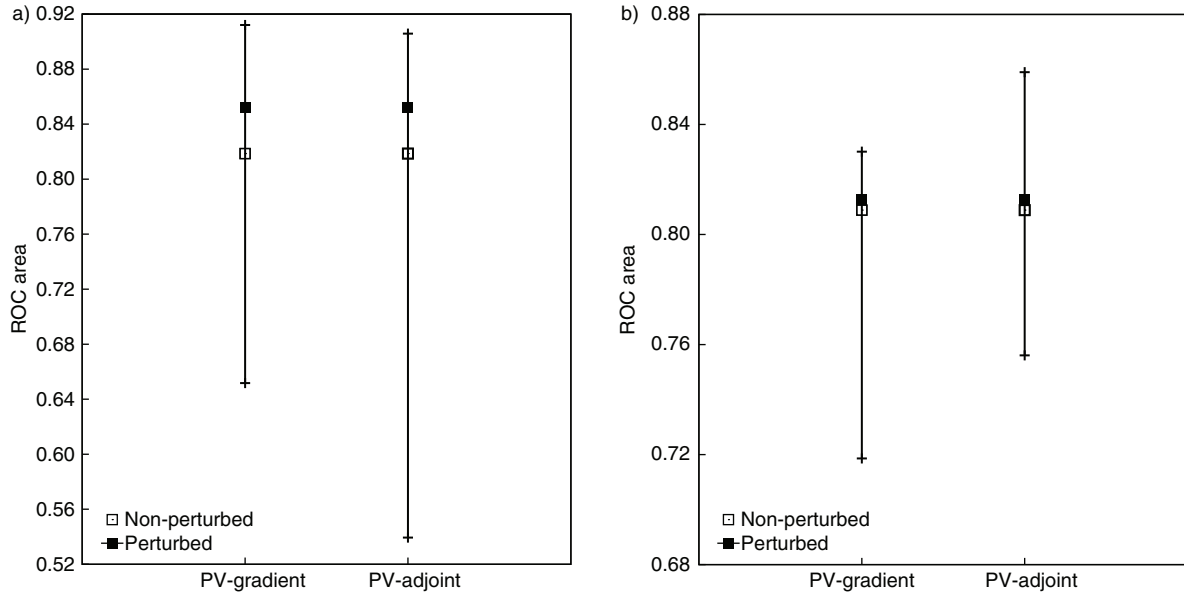
Fig. 10. ROC area range for the PV-gradient and PV-adjoint ensemble members, where the empty square corresponds to the non-perturbed run and the filled square to the PV-WV perturbed run. (a) June 2000 event and (b) October 2002 case. The vertical lines represent these ROC area ranges where the extremes, maximum and minimum, of the range correspond to the ensemble member associated with the highest/lowest value of ROC area.

elongated than the October 2002 cluster of positions, meaning that almost all June 2000 runs exhibit an RMS difference around 9 mm, while the RMS difference shown by the October 2002 runs ranges from 8 to 18 mm. Another difference between the cases is in the correlation coefficient; on the June 2000 events it ranges from 0.4 to 0.7, higher values than those obtained for the October 2002 event (from 0.15 to 0.55). Even though the observed precipitation field is different in each event, both exhibit a similar standard deviation almost 10 mm on the June 2000 event and around 9 mm on the October 2002 case. The standard deviations of forecasts range from 0 to 15 mm for the June 2000 case and from 8 to 18 mm for the October 2002 event. It is also worth mentioning that the statistics displayed on the Taylor diagram are negatively affected by the discontinuities, noise and outliers typically present in the rainfall field.

5. Concluding remarks and future outlook

This paper implements a PV modifying technique applied to the initial state of two Mediterranean high-impact weather events and tests its impact on the corresponding mesoscale forecasts. The applied technique is based on correcting the mismatch between the upper-level PV field and the observed WV brightness temperature given by the METEOSAT-7 satellite. The forecast precipitation fields, our feature of interest because of its regional socio-economical impact, obtained after perturbing the initial

state show a clear improvement compared with the non-perturbed forecast, even though still there seems to be room for improvement in the two selected events.

The examined verification scores also reflect the improvement in skill when the initial state of the event is perturbed using the PV-WV technique described in this study. In fact this improvement is observed in both events, and on all the verification scores presented, the perturbed run always achieves a higher score than the non-perturbed run. When the perturbed and non-perturbed runs are compared with the PV-adjoint and PV-gradient ensemble members, they remain within the range of both EPS members' scores and are statistically indistinguishable from the ensemble members. In this study, the PV-WV technique was used aiming for the best subjective modification, but it could also be applied to generate a larger spread from an ensemble generation perspective by introducing high amplitude modifications, always with the ultimate goal of improving the match between PV field and WV brightness temperature. Therefore, it would be worth trying to generate a pseudo-ensemble based on the PV-WV technique implementing different manual perturbations by one or several forecasters, taking advantage of the uncertainty present on the initial state and the subjectivity implicit in the method. The value of human-generated perturbations in an ensemble forecasting framework has already been explored by Homar et al. (2006) with satisfactory results. In fact, this study showed that an EPS clearly benefits from human contribution and
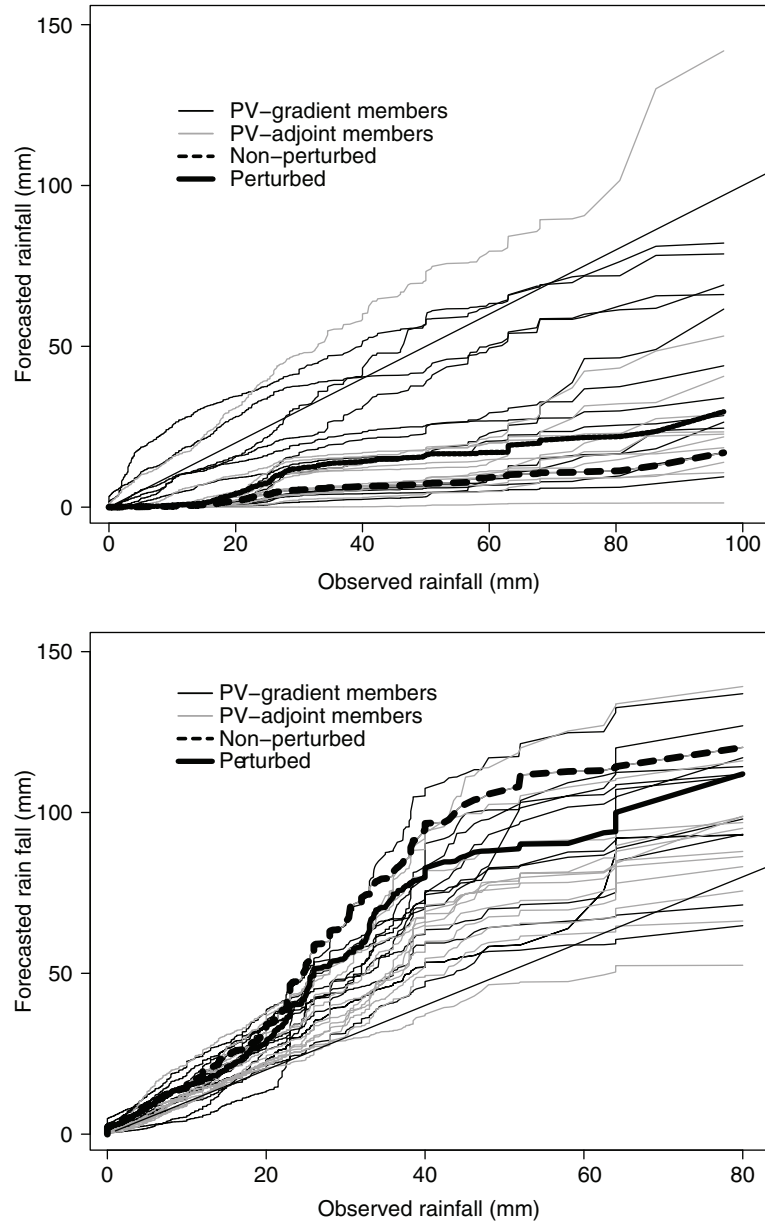
Fig. 11. Q-Q plot for the PV-gradient and PV-adjoint ensemble members, where the dashed line corresponds to the non-perturbed run and the dotted line to the PV-WV perturbed run. (a) June 2000 event and (b) October 2002 case.

suggested further experiments to improve our knowledge of how to take advantage of the forecasters' experience when building an EPS. The proposed pseudo-ensemble will provide more results on the forecasters' role in successfully generating ensemble prediction systems.

Having these results in mind, the next step should be to compare the PV-WV technique run with each ensemble member individually, in order to evaluate the strengths and weaknesses of the presented technique compared with the perturbed states obtained with the EPSs. It is also worth exploring whether, statistically (i.e. over a large number of

events), the PV-WV technique outputs lie systematically within the range of the best ensemble members and whether this technique can be used to generate new ensemble members that would lead to greater spread. Note that the PV-WV subjective technique would provide the ensemble members with that sample analysis error probability density function using the observations as guidance, so while objective ensemble generation methods like the PV-gradient and PV-adjoint methods may fail; if there is a significant difference between the initial state (e.g. analyses) and the observations, the PV-WV technique would be very
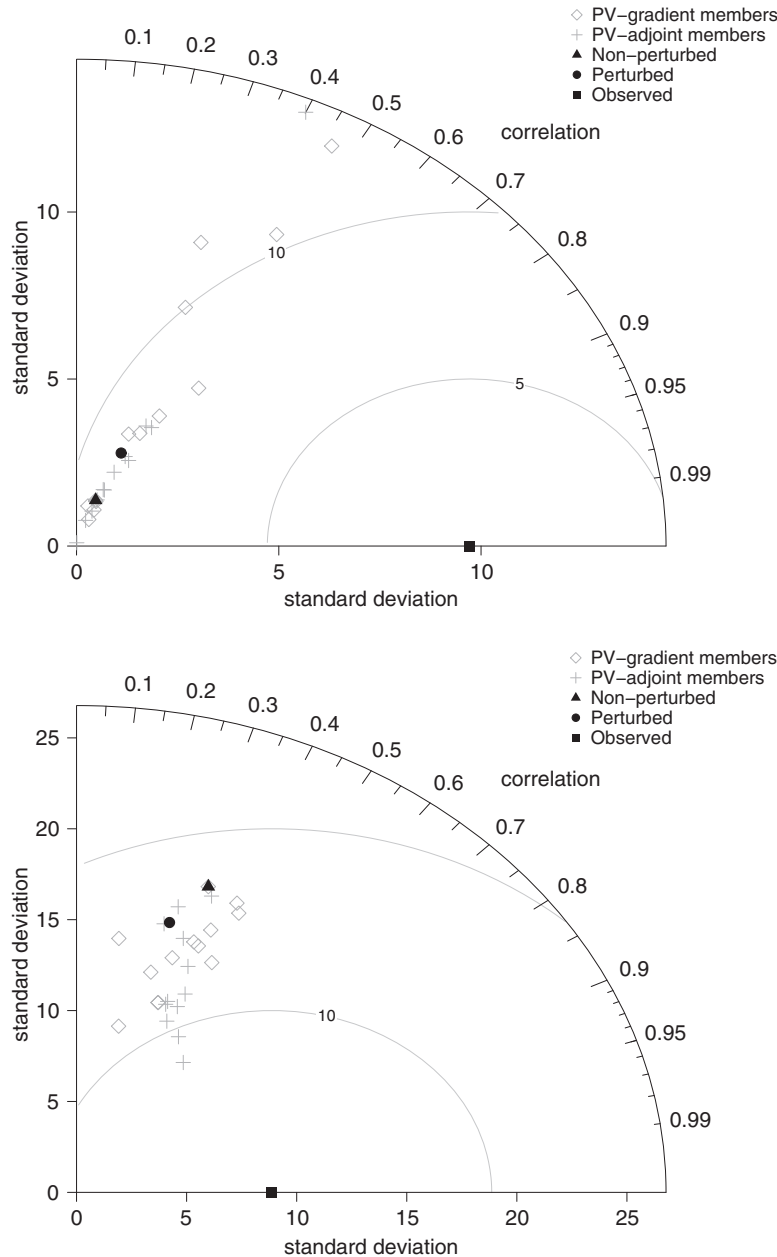
Fig. 12.   Taylor diagram for the PV-gradient and PV-adjoint ensemble members, where the solid triangle corresponds to the non-perturbed run, the solid circle to the PV-WV perturbed run and the solid square to the observations. (a) June 2000 event and (b) October 2002 case. The radial distance from the origin is proportional to the standard deviation of a pattern. The centred RMS difference between the observed and forecast field is proportional to their distance apart. The correlation between the two fields is given by the azimuthal position of the forecast field. The standard deviation and centred RMS difference units are rainfall in millimetres. The perfect score is obtained when the data point representing the forecast field matches up with the observed one.

beneficial to the global ensemble in these special situations. In this sense, repeating these kinds of experiments for the whole set of MEDEX cases used in the study of Vich et al. (2011a, 2011b) for both ensemble generation methods – subjective and objective – would expand the test bed explored in this paper and may allow to extract more general and robust conclusions. Moreover, the forthcoming HyMeX 2012 Special Observation Period (SOP) campaign (see http://www.hymex.org for details) will provide an excellent real-time framework to further explore the capabilities and application of perturbation techniques like the ones studied in this paper.

6. Acknowledgements

References

Arbogast, P., Maynard, K. and Piriou, C. 2012. About the reliability of manual model PV corrections to improve forecasts. *Weather Forecast*. DOI: 10.1175/WAF-D-11-00110.1

Argence, S., Lambert, D., Richard, E., Chaboureau, J.-P., Arbogast, P. and co author. 2009. Improving the numerical prediction of a cyclone in the Mediterranean by local potential vorticity modifications. *Quart. J. Roy. Meteor. Soc.* **135**, 865–879. DOI: 10.1002/gj.

Charney, J. G. 1955. The use of primitive equation of motion in numerical prediction. *Tellus* **7**, 22–26.

Dermitas, M. and Thorpe, A. 1999. Sensitivity of short-range weather forecasts to local potential vorticity modifications. *Mon. Weather Rev.* **127**, 922–939.

Dudhia, J. 1989. Numerical study of convection observed during the winter monsoon experiment using a mesoscale two-dimensional model. *J. Atmos. Sci.* **46**, 3077–3107.

Dudhia, J. 1996. A multi-layer soil temperature model for mm5. *Preprints from the Sixth PSU/NCAR Mesoscale Model Users' Workshop 22–24*. Online at: http://www.mmm.ucar.edu/mm5/lsm/soil.pdf.

Garcies, L. and Homar, V. 2009. Ensemble sensitivities of the real atmosphere: application to Mediterranean intense cyclones. *Tellus A* **61**, 394–406. DOI: 10.1111/j.1600-0870.2009.00392.x.

Guérin, R., Desroziers, G. and Arbogast, P. 2006. 4D-Var analysis of potential vorticity pseudo-observations. *Quart. J. Roy. Meteor. Soc.* **132**, 1283–1298.

Hello, G. and Arbogast, P. 2004. Two different methods to correct the initial conditions applied to the storm of 27 December 1999 over southern France. *Meteor. Appl.* **11**, 51–57.

Homar, V., Romero, R., Stensrud, D. J., Ramis, C. and Alonso, S. 2003. Numerical diagnosis of a small, quasi-tropical cyclone over the Western Mediterranean: dynamical vs. boundary factors. *Quart. J. Roy. Meteor. Soc.* **129**, 1469–1490.

Homar, V. and Stensrud, D. J. 2004. Sensitivities of an intense Mediterranean cyclone: analysis and validation. *Quart. J. Roy. Meteor. Soc.* **130**, 2519–2540.

Homar, V., Stensrud, D. J., Levit, J. J. and Bright, D. R. 2006. Value of human-generated perturbations in short-range ensemble forecasts of severe weather. *Weather Forecast*. 21, 347. DOI: 10.1175/WAF920.1.

Hong, S.-Y. and Pan, H.-L. 1996. Nonlocal boundary layer vertical diffusion in a medium-range forecast model. *Mon. Weather Rev.* **124**, 2322–2339.

Hoskins, B. J., McIntyre, M. E. and Robertson, A. W. 1985. On the use and significance of isentropic potential vorticity maps. *Quart. J. Roy. Meteor. Soc.* **111**(470), 877–946.

Houtekamer, P. L., Lefaivre, L., Derome, J., Ritcie, H. and Mitchell, H. L. 1996. A system simulation approach to ensemble prediction. *Mon. Weather Rev.* **124**, 1225–1242.

Huo, Z., Zhang, D.-L. and Gyakum, J. 1999. Interaction of potential vorticity anomalies in extratropical cyclogenesis. Part I: static piecewise inversion. *Mon. Weather Rev.* **127**, 2546–2560.

Kain, J. S. 2004. The Kain-Fritsch Convective Parameterization: an update. *J. Appl. Meteor.* **43**, 170–181.

Lorenz, E. N. 1963. Deterministic nonperiodic flow. *Atmos. Sci.* **20**, 130–141.

Manders, A., Verkley, W., Diepeveen, J. and Moene, A. 2007. Application of a potential vorticity inversion method to a case of rapid cyclogenesis over the Atlantic Ocean. *Quart. J. Roy. Meteor. Soc.* **133**, 1755–1770.

Martín, A., Romero, R., Homar, V., De Luque, A., Alonso, S., and co authors. 2007. Sensitivities of a flash flood event over Catalonia: a numerical analysis, *Mon. Weather Rev.* **135**, 651–669.

Mason, I. 1982. A model for assessment of weather forecasts. *Aust. Meteorol. Mag.* **30**, 291–203.

Meng, Z. and Zhang, F. 2007. Tests of an ensemble Kalman filter for mesoscale and regional-scale data assimilation. Part II: imperfect model experiments. *Mon. Weather Rev.* **135**, 1403–1423.

Nuissier, O., Ducroq, V., Ricard, D., Lebeaupin, C. and Anquetin, S. 2007. A numerical study of three catastrophic events over Southern France. Part I: numerical framework and synoptic ingredients. *Quart. J. Roy. Meteor. Soc.* **134**, 11–130.

Nutter, P. A., Mullen, S. L. and Baumhefner, D. P. 1998. The impact of initial condition uncertainty on numerical simulations of blocking. *Mon. Weather Rev.* **126**, 2482–2502. DOI: 10.1175/1520-0493(1998)126¡2482:TIOICU¿2.0.CO;2.

Rabier, F., Klinker, E., Courtier, P. and Hollingsworth, A. 1996. Sensitivity of forecast errors to initial conditions. *Quart. J. Roy. Meteor. Soc.* **122**, 121–150. DOI: 10.1002/qj.49712252906.

Reisner, J., Rasmussen, R. and Bruintjes, R. 1998. Explicit forecasting of supercooled liquid water in winter storms using the mm5 mesoscale model. *Quart. J. Roy. Meteor. Soc.* **124**, 1071–1107. DOI: 10.1002/qj.49712454804.

Romero, R. 2001. Sensitivity of a heavy rain producing Western Mediterranean cyclone to embedded potential vorticity anomalies. *Quart. J. Roy. Meteor. Soc.* **127**, 2559–2597.

Romero, R. 2008. A method for quantifying the impacts and interactions of potential-vorticity anomalies in extratropical cyclones. *Quart. J. Roy. Meteor. Soc.* **134**, 385–402.

Romero, R., Doswell III, C. A. and Ramis, C. 2000. Mesoscale numerical study of two cases of long-lived quasistationary convective systems over eastern Spain. *Mon. Weather Rev.* **128**, 3731–3751.

Romero, R., Martín, A., Homar, V., Alonso, S. and Ramis, C. 2005. Predictability of prototype flash flood events in the

western Mediterranean under uncertainties of the precursor upper-level disturbance: the HYDROPTIMET case studies. *Nat. Haz. and Earth. Syst. Sci.* **5**, 505–525.

Romero, R., Martín, A., Homar, V., Alonso, S. and Ramis, C. 2006. Predictability of prototype flash flood events in the western Mediterranean under uncertainties of the precursor upper-level disturbance: the HYDROPTIMET case studies. *Adv. Geosci.* **7**, 55–63.

Røsting, B. and Kristjánson, J. 2006. Improving simulations of severe winter storms by initial modification of potential vorticity in sensitive regions. *Quart. J. Roy. Meteor. Soc.* **132**, 2625–2652.

Røsting, B. and Kristjánson, J. 2008. A successful resimulation of the 7–8 January 2005 winter storm through initial potential vorticity modification in sensitive regions. *Tellus* **60A**, 604–619.

Santurette, P. and Georgiev, C. G. 2005. Weather analysis and forecasting: applying satellite water vapor imagery and potential vorticity analysis. Academic Press, London, 200 pp., ISBN: 9780126192629.

Santurette, P. and Joly, A. 2002. ANASYG/PRESYG, Météo-France's new graphical summary of the synoptic situation. *Meteor. Appl.* **9**, 129–154.

Stensrud, D., Brooks, H., Du, J., Tracton, M. and Rogers, E. 1999. Using ensembles for short-range forecasting. *Mon. Weather Rev.* **127**, 433–446.

Stensrud, D. and Yussouf, N. 2007. Reliable probabilistic quantitative precipitation forecasts from a short-range ensemble forecasting system. *Weather Forecast.* **22**, 3–17.

Taylor, K. E. 2001. Summarizing multiple aspects of model performance in a single diagram. *J. Geophys. Res.* **106**, 7183–7192.

Troen, I. and Mahrt, L. 1986. A simple model of the atmospheric boundary layer: sensitivity to surface evaporation. *Bound-Lay Meteorol.* **37**, 129–148.

Vich, M., Romero, R. and Brooks, H. E. 2011a. Ensemble prediction of Mediterranean high-impact events using potential vorticity perturbations. Part I: comparison against the multi-physics approach. *Atmos. Res.* **102**, 227–241. DOI: 10.1016/j.atmosres.2011.07.017.

Vich, M., Romero, R. and Homar, V. 2011b. Ensemble prediction of Mediterranean high-impact events using potential vorticity perturbations. Part II: adjoint-derived sensitivity zones. *Atmos. Res.* **102**, 311–319. DOI: 10.1016/j.atmosres.2011.07.016.

Wilks, D. S. 1995. Statistical methods in the atmospheric sciences: an introduction. In: *International Geophysics Series* (ed. D. S. Wilks) Vol. 59, Academic Press, London, 467 pp., ISBN: 0127519653.